Cylinder↔sphere epitaxial transitions in block copolymer melts

M. W. Matsen
Polymer Science Centre, University of Reading, Whiteknights, Reading RG6 6AF, United Kingdom

(Received 13 December 2000; accepted 21 February 2001)

We examine the Landau free energy surface of a diblock copolymer melt using self-consistent field theory. The topography of its surface is found to exhibit a low-energy pathway connecting the local minima associated with the cylindrical (C) and spherical (S) morphologies. The pathway corresponds to an epitaxial transition where the periodicity of the two phases is matched with the cylinder axis oriented in one of the [111] directions of the bcc spheres. The energy barriers and stability limits are evaluated, and from them we conclude that the C↔S transition should normally occur by a nucleation and growth mechanism. Based on the generally small energy barriers, we suggest that fluctuation effects are much stronger than previously anticipated. Furthermore, we examine the way the morphology evolves during a transition and discuss its signature in a small-angle scattering experiment. © *2001 American Institute of Physics.*
[DOI: 10.1063/1.1365085]

I. INTRODUCTION

Block copolymer melts have become one of the preferred systems for studying phenomena associated with molecular self-assembly.[1] Most favored is the simple AB diblock architecture, where a polymer chain of fN segments denoted A and a second chemically distinct chain of $(1-f)N$ segments denoted B are joined together by their ends to form a single molecule. Its mean-field phase diagram,[2] shown in Fig. 1, is in excellent agreement with experiment,[1] and as a result we have a thorough understanding of its equilibrium phase behavior.[3] The product χN of the Flory–Huggins interaction parameter and the total degree of polymerization controls the tendency of the A and B blocks to separate. At sufficiently large values (i.e., $\chi N \gtrsim 10$), the A and B blocks microphase separate forming a periodically ordered microstructure.[4] The periodicity is determined by a competition between the interfacial tension and the entropic loses of deforming (i.e., stretching) the polymers.[5] A further competition between the stretching energies of the A and B blocks creates a spontaneous interfacial curvature, where the smaller block is favored on the inside of the curvature.[5] For similar sized blocks (i.e., $f \approx 0.5$), the spontaneous curvature is approximately zero and consequently the system forms a lamellar (L) phase with flat interfaces. As the blocks become asymmetric, the spontaneous curvature increases in magnitude causing transformations to the gyroid (G), cylindrical (C), and spherical (S) morphologies. The finer details of the behavior are controlled by the ability of morphologies to simultaneously produce uniform interfacial mean curvature and uniform domain thickness, so as to further minimize the interfacial and stretching energies, respectively.[3,6] The inability of various phases, such as perforated-lamellae (PL), to do so prevents them from being stable.[7] This *packing frustration* is also responsible for the cylindrical and spherical microdomains of the C and S phases ordering into hexagonal and bcc lattices, respectively.[8] Although theory predicts a narrow close-packed spherical (S_{cp}) region, this is attributed to a significant population of *free* chains in the matrix domain resulting when the minority block becomes ineffective in anchoring the molecule to the interface.[6]

The mean-field theory is generally accurate for block copolymer melts primarily because the large size of these macromolecules suppresses fluctuation effects. Nevertheless, there are two situations where thermal fluctuations significantly alter the phase diagram in Fig. 1. Based on experiments,[9–11] they disrupt the long-range order in the S_{cp} phase transforming it into part of the disordered region. Secondly, Brazovskii-type fluctuations[12] destroy the weakly-ordered structures near $\chi N \approx 10$ shifting the order–disorder transition (ODT) upwards. According to a weak-segregation calculation,[13] the shift at $f=0.5$ is given by $\chi N = 10.495 + 41.022\bar{N}^{-1/3}$, where $\bar{N} \equiv \rho_0^2 a^6 N$ is the invariant polymerization index.

Given this solid theoretical understanding, diblock copolymer melts represent an ideal system for examining phase transitions between periodically-ordered phases. So far, the most studied order–order transition in block copolymer melts is between hexagonal cylinders and bcc spheres.[9,10,14–24] This reversible transition was first identified by Sakurai *et al.*[14] in 1993. Soon after, Koppi *et al.*[15] provided evidence that the transition occurs by means of the epitaxial pathway illustrated in Fig. 2. As C transforms into S, each cylinder pinches off with a periodicity $D_\parallel$ into a series of spheres. The spheres form hexagonally-packed layers perpendicular to the cylinder axis with an in-layer spacing of $D_\perp$ and an out-of-layer spacing of $D_\parallel/3$. The stacking repeats every three layers in either an ABCABC… or an ACBACB… sequence; the two possibilities lead to a twinned bcc microstructure. This epitaxy has been confirmed to occur in both directions, C↔S, by more recent experiments.[16] Interestingly, lyotropic liquid crystal systems exhibit the exact same epitaxial transitions between their cylindrical and spherical phases,[25] as is the case with the C↔G transitions.[26]

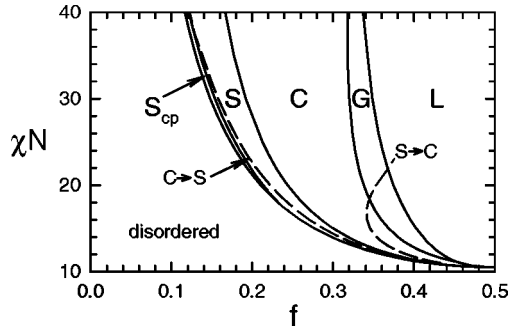

FIG. 1. Mean-field phase diagram for AB diblock copolymers plotted in terms of segregation χN and composition f. The ordered phases are lamellar (L), gyroid (G), cylindrical (C), spherical (S), and closed-packed spherical (S_{cp}). The dashed curves are the spinodal lines for the C↔S epitaxial transitions.

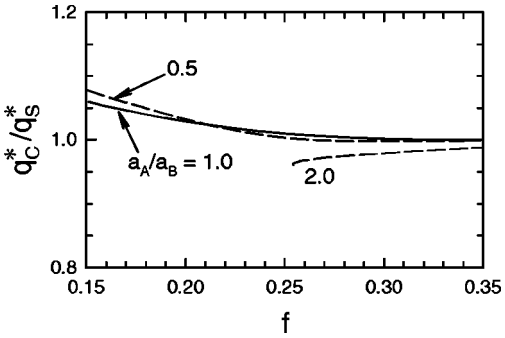

FIG. 3. The ratio q_C^*/q_S^* of the principal scattering vectors of the C and S phases calculated along the C/S phase boundary. The solid and dashed curves are for conformationally symmetric and asymmetric copolymers, respectively.

A clear signature of the C↔S epitaxial mechanism is that the cylinder axis of the C phase coincides with the [111] direction of the bcc S phase. However, the epitaxy also requires the ratio $D_\parallel/D_\perp$ to equal, at least approximately, $3/\sqrt{8}=1.06066\ldots$. This happens to correspond to a match in the principal scattering vectors, q_S^* and q_C^*, of the two phases. The theoretical prediction for the ratio q_C^*/q_S^*, shown in Fig. 3, is indeed close to one, at least for diblock copolymer melts. This is also consistent with most experimental observations,[9,15,17–19] although there are some systems where the deviation from one reaches $\sim 10\%$.[14,20]

There have been a number of theoretical approaches used to examine order–order transitions (OOT's) in block copolymer melts.[27] Qi and Wang[28] examined pathways between ordered morphologies using a generic Landau–Ginzburg free energy functional and then later[29] the more specific Leibler free energy functional.[4] However, their approach is limited to large temperature jumps beyond the spinodal limits of the initial phase. Later Laradji *et al.*[30,31] performed a stability analysis for the various ordered phases using an exact mean-field Landau free energy functional. From the lowest energy modes, they inferred a number of epitaxial pathways. Shi and Noolandi have since repeated the calculation for a simpler Landau–Ginzburg free energy functional.[32] All of these calculations suffer from limitations restricting them to weak segregations, where the ordered phases are destroyed by thermal fluctuations.[13] More recently, we introduced a SCFT calculation[26] capable of examining the exact mean-field Landau free energy surface at far higher degrees of segregation, where fluctuations are relatively unimportant and where the behavior is known[6] to obey the simple competition between interfacial and stretching energy described above. Furthermore, this method can explore the entire pathway between two given phases. Our first application[26] examined an epitaxial pathway between the C and G phases, results of which are now in good agreement with experiment.[33,34] Below, we perform analogous calculations for the epitaxial pathway between the C and S phases.

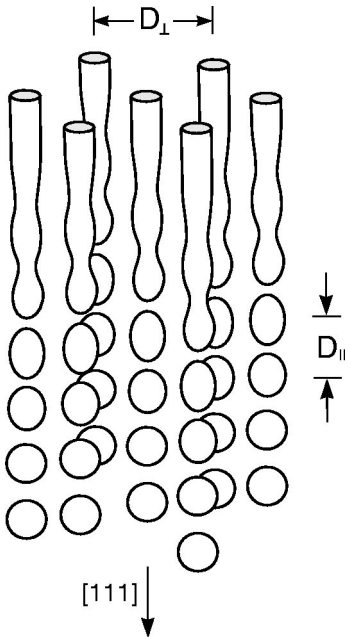

FIG. 2. Schematic diagram of the epitaxial transition between hexagonal cylinders (C) and body-centered-cubic spheres (S). The cylinder axis coincides with the [111] direction of the bcc lattice. The spacing between the cylinders is denoted as $D_\perp$, and the spacing of the spheres along the [111] direction is labeled as $D_\parallel$.

II. THEORY

The calculations presented in this paper are all performed using the standard flexible Gaussian chain model in conjunction with self-consistent field theory (SCFT).[35] A detailed study of AB diblock melts using this theory is presented in Ref. 6. The model system involves n identical molecules each with N segments of which a fraction f forms the A block. It is assumed that each segment occupies a fixed volume, ρ_0^{-1}, so that the total volume is $\mathcal{V}=nN/\rho_0$. The A–B segment interaction is controlled by the standard Flory–Huggins χ parameter. Although the theory allows for distinct A and B segment lengths, $a_A \neq a_B$,[36] we limit our attention to conformationally symmetric copolymers with $a_A=a_B\equiv a$.

In order to consider phase transitions, we construct a Landau free energy functional, $F[\Phi]$, that provides the free energy of the melt for a specified segment distribution, $\Phi(\mathbf{r})$. The distribution is defined so that the A and B segment profiles equal $\frac{1}{2}[1+\Phi(\mathbf{r})]$ and $\frac{1}{2}[1-\Phi(\mathbf{r})]$, respectively. In general, the Landau free energy surface possesses a compli-

cated topograph of peaks and valleys with each metastable phase corresponding to a local minimum. Evidently, many of these local minima are connected by low-lying pathways, where the energy rises up to a saddle point and then back down. When the melt is well segregated, the system evolves between the two different states by following such pathways, since this minimizes the energy barrier. Here, we will not be too concerned about the actual pathway so much as the size of the energy barrier. A rigorous treatment of the former is beyond the scope of this paper.

We calculate the Landau free energy $F[\Phi]$ following the SCFT method described previously in Ref. 26, where a field $w(\mathbf{r})$ is used to enforce the desired concentration profile. Conventional SCFT calculations can only locate the extrema in the Landau free energy surface, which generally correspond to stable or metastable states. In these cases, $w(\mathbf{r})=-\frac{1}{2}\chi N\Phi(\mathbf{r})$. Since saddle points are also extrema, they can be located as well. However, our more general calculation is required in order to examine the entire pathway between the two minima.

To make our calculation feasible at the intermediate segregations that are most relevant to experiments, we assume the system maintains a periodic morphology. Although this is not physically realistic, we will argue in the Discussion that the resulting pathways are closely related to actual experimental ones. Given this assumption, $\Phi(\mathbf{r})$ can be expanded as

$$\Phi(\mathbf{r})=2f-1+\sum_{i=1}^{\infty}\Phi_i f_i(\mathbf{r}), \tag{1}$$

where the basis functions, $f_i(\mathbf{r})$, each possess some appropriate symmetry and are normalized so that they form an orthonormal set satisfying

$$\frac{1}{\mathcal{V}}\int d\mathbf{r} f_i(\mathbf{r}) f_j(\mathbf{r})=\delta_{ij}. \tag{2}$$

The resulting set of coefficients, $\{\Phi_i\}$, defines the independent variables of the free energy functional, which is thus embedded in an infinite-dimensional space. For the $\underline{\mathrm{C}}\leftrightarrow\mathrm{S}$ transition, the appropriate space-group symmetry is R3m,[37] and thus the first few basis functions are

$$f_1(\mathbf{r})=\sqrt{2/3}[\cos(2X)+2\cos(X)\cos(3Y)], \tag{3}$$

$$f_2(\mathbf{r})=\sqrt{2/3}[\cos(2Y)\cos(Z)+2\cos(X)\cos(Y)\cos(Z) -\sin(2Y)\sin(Z)+2\cos(X)\sin(Y)\sin(Z)], \tag{4}$$

$$f_3(\mathbf{r})=\sqrt{2/3}[\cos(4Y)\cos(Z)+2\cos(2X)\cos(2Y)\cos(Z) -\sin(4Y)\sin(Z)+2\cos(2X)\sin(2Y)\sin(Z)], \tag{5}$$

$$f_4(\mathbf{r})=\sqrt{2/3}[\cos(6Y)+2\cos(3X)\cos(3Y)], \tag{6}$$

$$f_5(\mathbf{r})=\sqrt{2/3}[\cos(2Y)\cos(2Z)+2\cos(X)\cos(Y)\cos(2Z) +\sin(2Y)\sin(2Z)-2\cos(X)\sin(Y)\sin(2Z)], \tag{7}$$

$$f_6(\mathbf{r})=\sqrt{4/3}[\cos(3X)\cos(Y)\cos(Z) +\cos(2X)\cos(4Y)\cos(Z)+\cos(X)\cos(5Y)\cos(Z) +\cos(3X)\sin(Y)\sin(Z)+\cos(2X)\sin(4Y)\sin(Z) -\cos(X)\sin(5Y)\sin(Z)], \tag{8}$$

where $X\equiv 2\pi x/\sqrt{3}D_\perp$, $Y\equiv 2\pi y/3D_\perp$, and $Z\equiv 2\pi z/D_\parallel$. The functions are ordered with increasing wave vectors assuming a ratio $D_\parallel/D_\perp=3/\sqrt{8}$. Of course, it is impossible to consider the infinite set of basis functions, but we can at least manage 500. By truncating the set, we simply limit the degree of segregation that can be considered.

In many cases, it useful to expand the free energy functional about a particular segment profile $\Phi(\mathbf{r})$ as

$$\frac{F[\Phi+\delta\Phi]}{nk_BT}\approx\frac{F[\Phi]}{nk_BT}-\sum_i\left(\frac{1}{2}\chi N\Phi_i+w_i\right)\delta\Phi_i +\frac{1}{2}\sum_{ij}[\mathbf{C}_{\mathrm{RPA}}^{-1}]_{ij}\delta\Phi_i\delta\Phi_j, \tag{9}$$

where $\delta\Phi(\mathbf{r})$ is a small variation. It is also convenient to define a distance δs between $\Phi(\mathbf{r})$ and $\Phi(\mathbf{r})+\delta\Phi(\mathbf{r})$ using

$$[\delta s]^2\equiv\frac{1}{\mathcal{V}}\int d\mathbf{r}[\delta\Phi(\mathbf{r})]^2=\sum_i[\delta\Phi_i]^2. \tag{10}$$

The matrix $\mathbf{C}_{\mathrm{RPA}}$ is calculated as described in Ref. 26 following a procedure similar to that of Shi *et al.*[38] An extremum in the Landau free energy surface occurs when the linear term in $\delta\Phi(\mathbf{r})$ vanishes. The extremum represents a metastable state when all the eigenvalues of $\mathbf{C}_{\mathrm{RPA}}^{-1}$ are positive, whereas it is a saddle point if one of the eigenvalues is negative.

There are many possible pathways the system can take through the saddle point. We examine a reasonable one constructed in the following way. We first locate the saddle point approximately midway between the two phases of interest, and label it as $s=0$. We then evaluate the eigenvalues and eigenvectors of $\mathbf{C}_{\mathrm{RPA}}^{-1}$. The eigenvector associated with the negative eigenvalue defines two directions, one pointing towards C and the other towards S. We step a small distance, $\delta s=0.01$, in the latter direction and label the point as $s=0.01$. There we evaluate the expansion, Eq. (9), for $F[\Phi]$ and use it to find the lowest energy at a small fixed distance $\delta s=0.01$ away. This next point is labeled as $s=0.02$. The procedure is repeated until the local minimum corresponding to S is reached. The same procedure is then followed to obtain a pathway from the saddle point to C, but this time the parameter s is indexed with negative values. Our step size, δs, is chosen small enough so that the expansion in Eq. (9) remains accurate. Generally, we minimize $F[\Phi]$ with respect to the dimensions, $D_\parallel$ and $D_\perp$, at each step, but in a few cases the procedure is performed with fixed dimensions.

III. RESULTS

We begin by calculating the kinetic pathway from C to S at three points on the C/S phase boundary. The variation in energy along these pathways, shown in Fig. 4(a), is rather featureless. The energy increases monotonically from the C phase until the saddle point at $s=0$ is reached, past which it decreases monotonically. Note that both ends of the pathway are at the same energy because we are on the phase boundary. Figure 4(b) shows the variation in $D_\perp$ and $D_\parallel$ as the

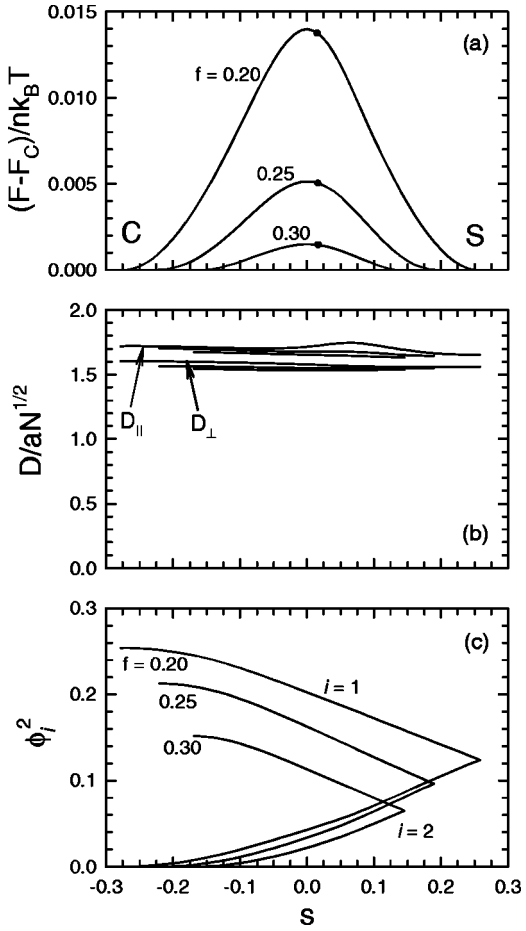

FIG. 4. (a) Variation in the free energy F as the C phase transforms into the S phase, at three different points on the C/S phase boundary. To compare the three curves, the free energy of the C phase F_C is subtracted. The parameter s, specifying the position along the pathway, is defined such that C occurs at $s<0$, the maximum energy corresponds to $s=0$, and the S phase occurs at $s>0$. Dots denote the points at which the cylinders rupture. (b) Variation in the cylinder spacing $D_{\|}$ and wavelength of its modulations $D_{\perp}$ as C transforms into S. (c) Square of the first two Fourier coefficients, Φ_1^2 and Φ_2^2, which are responsible for the principal peaks in a small-angle scattering experiment.

pathway is traversed. As required for epitaxial transitions, the domain spacings remain relatively constant. We also plot in Fig. 4(c) the square of the first two Fourier coefficients, Φ_1^2 and Φ_2^2, because they are proportional to the principal peaks in a small-angle scattering experiment. Starting in the C phase, Φ_1^2 is large while $\Phi_2^2=0$. As C evolves towards S, Φ_1^2 decreases while Φ_2^2 increases, until finally $\Phi_1^2=\Phi_2^2$ in the S phase.

Since the calculation provides all the Fourier coefficients Φ_i (up to some large cutoff), we have detailed information regarding how the morphology evolves along the pathway. Figure 5 shows the evolution of a single cylinder pinching off into a series of spheres for the intermediate pathway considered in Fig. 4. [The A/B interface is defined by $\Phi(\mathbf{r})=0$.] In this case, the cylinders rupture at $s=0.0163$ just to the S side of the saddle point. The points of rupture are indicated in Fig. 4(a) by solid dots.

The energy difference between the saddle point and the two equilibrium phases defines an energy barrier, ΔE, which

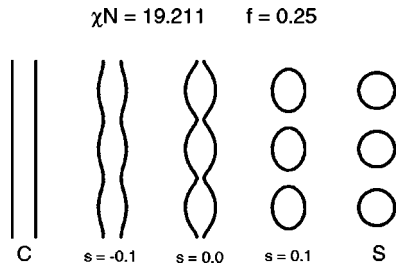

FIG. 5. Evolution of a single cylinder transforming into a series of spheres calculated for the intermediate path examined in Fig. 4(a). The interface is defined by $\Phi(\mathbf{r})=0$.

the system must overcome in order for the transition to proceed. Figure 6(a) plots this energy barrier per molecule as a function of f following the C/S phase boundary. A more meaningful gauge of the barrier is provided in Fig. 6(b) by plotting the energy in terms of the number of ruptures,

$$n_r = n\frac{2}{(3\bar{N})^{1/2}}\frac{a^3N^{3/2}}{D_{\perp}^2 D_{\|}}, \tag{11}$$

where $\bar{N}\equiv a^6\rho_0^2 N$ is the invariant polymerization index. Typical values of $\bar{N}$ range from 10^3 to 10^4.[39] With this, we can determine the energy per rupture (or fusion) in units of k_BT. Of course, values less than one k_BT imply that the barrier is insignificant compared to the thermal fluctuations.

Figure 7 is similar to Fig. 4, but it examines the kinetic pathway off of the C/S phase boundary for a series of segregations at a fixed composition, $f=0.25$. At this composition, S has a lower energy than C for $\chi N<19.211$, and vice versa for larger segregations. The variation in energy is again rather featureless; the only significant difference compared to

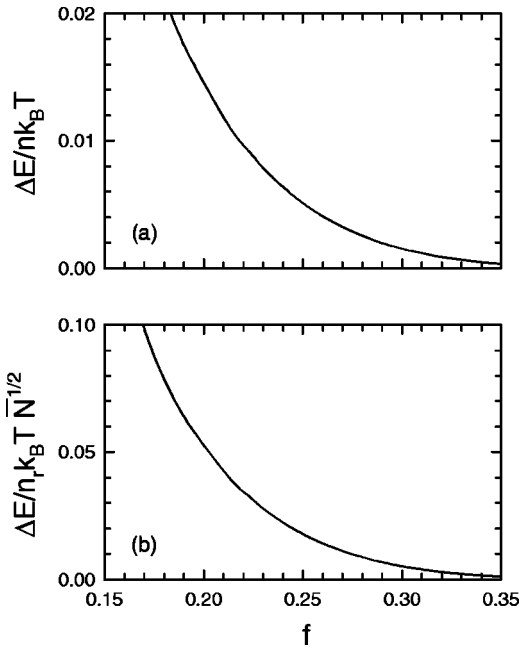

FIG. 6. Energy barrier ΔE of the C↔S transition plotted along the C/S phase boundary. The top plot (a) shows the energy per molecule, and the lower one (b) shows it per rupture. Typical values of the invariant polymerization index $\bar{N}$ range from 10^3 to 10^4 (Ref. 39).

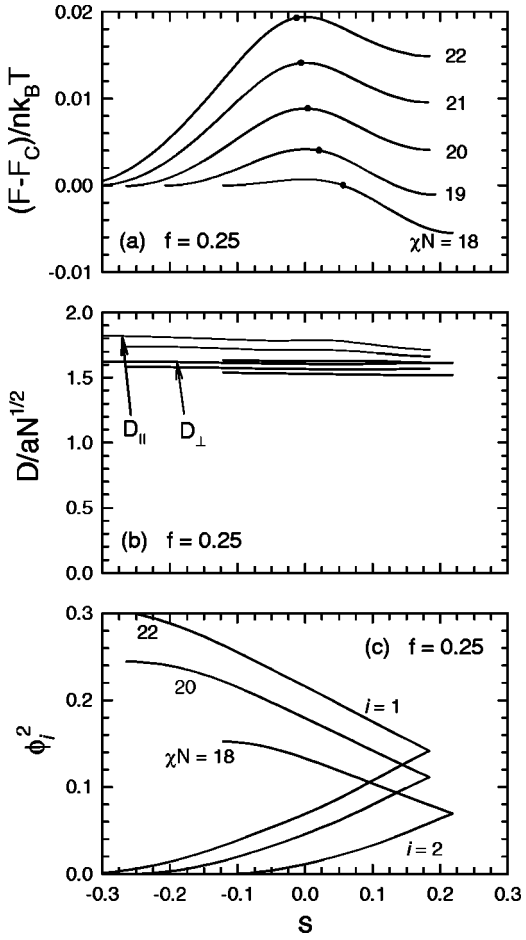

FIG. 7. Similar to Fig. 5, but calculated for a fixed composition $f=0.25$ at different degrees of segregation χN. Plots (b) and (c) only display results for the even values of χN.

Fig. 4(a) is that the two ends of the pathway are now at different energies. As before, Fig. 7(b) shows that the domain spacing remains relatively constant along the pathways as required for epitaxial transitions. Furthermore, Fig. 7(c) shows a similar variation in the predicted intensity of the principal scattering peaks.

For pathways off the phase boundary, there are two distinct energy barriers, $\Delta E_{C\to S}\equiv F_{\text{saddle}}-F_C$ and $\Delta E_{S\to C}\equiv F_{\text{saddle}}-F_S$, for the two different directions. These are plotted in Fig. 8 as a function of segregation χN, at compositions $f=0.20$, 0.25, and 0.30. At segregations below the phase boundary, we plot the barrier $\Delta E_{C\to S}$ preventing a metastable C phase from transforming into the stable S phase, and above we plot $\Delta E_{S\to C}$ for the reverse transition. Even though these curves join together (i.e., $\Delta E_{C\to S}=\Delta E_{S\to C}$) at the phase boundary, the boundary is clearly evident by the occurrence of a sharp kink. The solid curves are obtained by allowing the domain spacing to vary as the pathway is traversed, while the dashed ones are calculated holding $D_\perp$ and $D_\parallel$ constant so as to enforce a perfect epitaxial transition. Of course, this constraint increases the energy barrier, but only slightly in this case.

Figures 7(a) and 8 show that $\Delta E_{C\to S}\to 0$ as χN decreases. The C→S spinodal line plotted in Fig. 1 with a dashed curve specifies where the energy barrier first disappears. Beyond this curve, the C phase becomes absolutely unstable. Likewise, there is a spinodal line for the S→C transition also plotted in Fig. 1 with a dashed curve. However, this curve does not extend below $f=0.341$, which is why $\Delta E_{S\to C}$ does not tend to zero with increasing segregation for those compositions considered in Fig. 8.

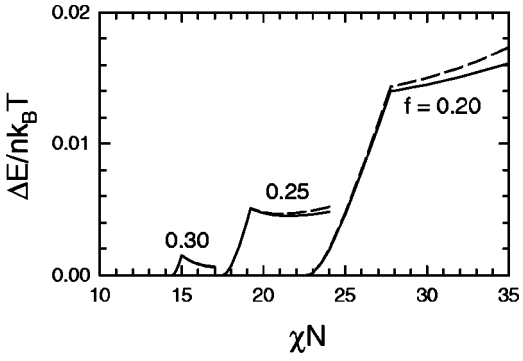

FIG. 8. Energy barriers, $\Delta E_{S\to C}$ and $\Delta E_{C\to S}$, plotted above and below the C/S phase boundary, respectively, as a function of segregation at three different compositions. The phase boundary is easily identified by the kinks where $\Delta E_{S\to C}$ and $\Delta E_{C\to S}$ join together. The solid and dashed curves correspond to calculations for varying and fixed domain sizes, respectively.

The effect of fluctuations on a metastable phase can be assessed by examining the eigenvalues of $\mathbf{C}_{\text{RPA}}^{-1}$.[38] In particular, the dominant fluctuation mode is specified by the eigenvector associated with the smallest eigenvalue, $\lambda_{\min}$. Not surprisingly, this mode generally coincides with the direction of the epitaxial pathway. Furthermore, the disappearance of the energy barrier coincides with $\lambda_{\min}\to 0$, which provides the most convenient way of determining the spinodal lines.

In the C phase, the dimension $D_\parallel$ can assume any value, and thus we need to examine $\lambda_{\min}$ vs $D_\parallel$ as shown in Fig. 9(a). The lowest value $\lambda_{\min}^*$ defines the dominant wavelength $D_\parallel^*$ for the cylinder fluctuations. Figure 9(b) shows the variation in $D_\parallel^*$ relative to the cylinder spacing along the C/S phase boundary and the spinodal line where $\lambda_{\min}^*=0$. In both cases, the ratio $D_\parallel^*/D_\perp$ only deviates slightly from $3/\sqrt{8}=1.060\,66\ldots$.

So far, we have assumed that the C and S phases acquire their preferred or equilibrium dimensions. However, it can take a considerable time for the domain spacing to adjust, and thus in real experiments morphologies are often slightly strained. To access how this affects the fluctuation modes, Fig. 10(a) plots $\lambda_{\min}$ for the S phase as a function of $D_\perp$ assuming $D_\parallel=(3/\sqrt{8})D_\perp$ as required for a bcc lattice. Similarly, Fig. 10(b) shows $\lambda_{\min}^*$ for the C phase as a function of $D_\perp$; the wavelength $D_\parallel^*$ of the preferred fluctuation is shown in the inset. Solid dots denote the equilibrium domain size. In both phases, straining the morphology can significantly enhance the fluctuations.

IV. DISCUSSION

Essential to an epitaxial transition is a good domain spacing match. If the periodicity of the morphology remains fixed, the transition can proceed with only a local rearrangement of the molecules. However, if the size of the unit cell is required to change, then a macroscopic transport of material

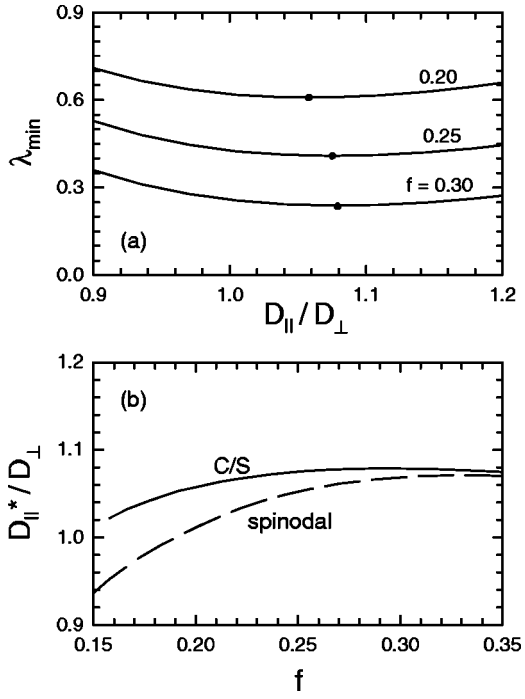

FIG. 9. (a) Stability of the cylinder (C) phase against fluctuations of wavelength $D_{\|}$ calculated at three compositions along the C/S phase boundary. Solid dots denote the dominant wave vector $D_{\|}^*$. (b) Wavelength $D_{\|}^*$ of the dominant fluctuation relative to the cylinder spacing $D_{\perp}$ calculated along the C/S phase boundary (solid curve) and along the C→S spinodal (dashed curve).

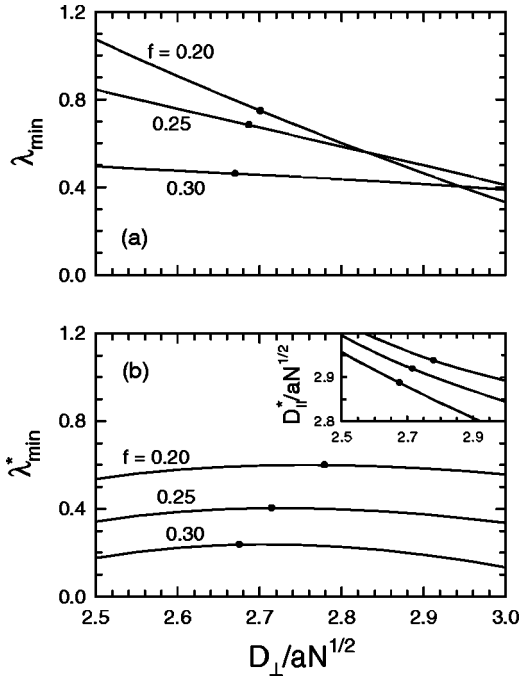

FIG. 10. Smallest eigenvalue of the $\mathbf{C}_{\mathrm{RPA}}^{-1}$ matrix, Eq. (9), as a function of domain spacing $D_{\perp}$ for the (a) S and (b) C phases calculated at three different compositions along the C/S phase boundary. Solid dots denote the equilibrium domain spacing. For the S phase, $D_{\|}$ is set to $3D_{\perp}/\sqrt{8}$, and for the C phase, $D_{\|}$ is set to the preferred wavelength $D_{\|}^*$ shown in the inset.

is necessary. Although, there exists a natural tendency for the equilibrium periodicities of C and S to match, there will always be some degree of mismatch which will vary from system to system. In the case of a small mismatch (i.e., $\lesssim 5\%$), the domain spacing will likely adjust as the morphology evolves from one phase to the other. Kim *et al.*[9] as well as Ryu and Lodge[17] observed this to occur gradually for the S→C transition, but abruptly for the C→S direction. It is uncertain why this happened and whether or not it is a general feature of this particular epitaxy. For a large mismatch (i.e., $\gtrsim 10\%$), the transition may occur in a two step process, where the morphology changes with a relatively fixed periodicity followed by a slow relaxation to the equilibrium domain size. Requiring the morphology to change with a fixed domain spacing will naturally increase the energy barrier, further impeding the transition. This has already been suggested as an explanation why in same cases the transition is unusually slow.[17,18,20] Undoubtedly, whatever happens will be significantly influenced by the population of defects and grain boundaries as they are presumably the sinks and sources for the material required to vary the domain size.

An epitaxial transition also requires an orientational match between the two phases, although it is by no means unique. Starting from a monodomain of C, there are two possible orientations of the S phase as discussed in the Introduction, and thus a polycrystalline morphology is produced with *twinned* bcc lattices. In the reverse direction, a monodomain of S forms a polycrystalline C phase with four different cylinder axes corresponding to the diagonals of the bcc unit cell. If the transition begins from a twinned S phase, then seven cylinder orientations are expected. Despite the finite number of possible orientations, Kohtaro *et al.*[16] found that oriented samples taken quickly through the sequence C →S→C generally return to their original orientation. They speculated that this *memory* effect results due to a delay in the copolymer junctions redistributing uniformly as new interface is created. A more likely explanation is that the spheres originating from different cylinders are poorly correlated. Although the spheres created by a single cylinder are automatically well aligned and can immediately rejoin to form a straight cylinder, the spheres will be somewhat misaligned in the other directions thus impeding the formation of the alternative cylinder orientations. Of course, this memory effect will fade as the system spends a longer time in the intermediate S phase allowing the spheres to adopt a more accurate bcc arrangement. Further evidence for a poorly ordered S phase has been presented in Ref. 20, where a long delay was observed between the disappearance of peaks corresponding to an ordered C phase and the appearance of those for the ordered S phase. We note that Refs. 21 and 22 have presented TEM evidence showing the formation of poorly ordered spheres, but this is expected as their initial C phases were also poorly ordered.

The orientational relation that exists during an epitaxial C→S transition should produce a clear signature in a small-angle scattering experiment. Figure 11 illustrates the expected pattern for a monodomain of C, with the cylinder axis in the z direction, growing into a twinned S phase. The solid dots in the q_x–q_y plane denote the principal and second-order peaks of the initial C phase. The strength of the six principal peaks is proportional to Φ_1^2 plotted in Figs. 5(c) and

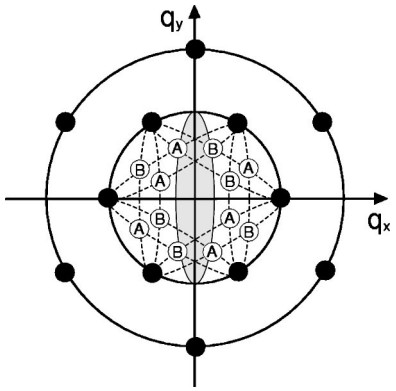

FIG. 11. Scattering peaks for an oriented C phase growing into a twinned bcc S phase (Ref. 17). The axes, chosen to be consistent with the basis functions in Eqs. (3)–(8), are oriented with the cylinder axis along the z direction pointing out of the page. Solid dots denote the principal and second-order scattering peaks of the C phase. The *A* and *B* positions show the additional principal peaks expected from the two twinned bcc lattices of the S phase. The shaded circle identifies the four principal peaks that should appear in the q_y–q_z plane as C transforms into S.

7(c). As the S phase grows, these peaks will decrease in intensity while new principal peaks proportional to Φ_2^2 appear at the locations mark as *A* and *B* in Fig. 11. The sets, *A* and *B*, correspond to the two twinned bcc structures. Assuming a polycrystalline S phase with equal populations of the twinned bcc lattices, the *A* and *B* peaks will attain equal intensities. The other principal peaks, corresponding to the original C phase, should finish with twice the intensity of the *A* and *B* peaks as they are common to both of the twinned lattices. Unfortunately, the S→C transition will not produce such a clear signature, because the resulting polycrystalline C phase generates the same set of principal peaks as the initial S phase.

Experiments have examined the Bragg reflections in Fig. 11 along three orthogonal planes. Kimishima *et al.*[16] have looked at the q_x–q_y plane from a single grain of the C phase. As expected, the peaks decrease in intensity with no new principal peaks emerging as the S phase grows in. Ryu *et al.*[17,18] have observed the q_y–q_z plane where none of the principal peaks and only two of the secondary peaks of the initial C phase are visible. Consistent with the shaded circle in Fig. 11, they observed the emergence of four new principal peaks each at 55° from the q_y axis. Although this is very compelling evidence for the epitaxial transition proposed in Fig. 2, experiments by Koppi *et al.*[15] and Krishnamoorti *et al.*[20] observe inconsistent results for the q_x–q_z plane where only two of the principal peaks and none of the secondary peaks of the initial C phase are visible. In this plane, no additional principal peaks should emerge, but nevertheless four new peaks like those expected for the q_y–q_z plane were clearly observed. The only reasonable explanation seems to be that their oriented C phase contained trace amounts of a second orientation rotated about the z axis by 90° with respect to the dominate orientation. In fact, both experiments[15,20] found evidence for this second orientation. Furthermore, this possibility is supported by recent results in Ref. 40. It should also be noted that the epitaxial relation between the G and C phases[33] was originally misreported because of a similar confusion regarding the orientation of the C phase.[41]

The way in which a C↔S transition proceeds depends strongly on the position of the spinodals plotted in Fig. 1. If the transition takes place between the two spinodals, then the initial phase is metastable and the transition should proceed by a nucleation and growth mechanism. In this case, the initial phase has to overcome an energy barrier ΔE, which it does by first forming a small critical nucleus of the equilibrium phase. In simple systems, the critical nucleus is the minimum size of the equilibrium phase required to compensate for the energy loss of forming a grain boundary between the two phases. In this more complicated transition, we can consider it as the smallest possible metastable change towards the stable phase. Once a metastable nucleus forms, it is unlikely to revert to the initial phase, and so it will continue to grow creating a single grain of the equilibrium phase. We note that defects can also act as nucleating sites. The final morphology will be a polycrystalline structure with approximately one grain for every critical nucleus that formed during the transition. If the energy barrier decreases, which happens as the spinodals are approached, more critical nuclei will be formed resulting in smaller grain sizes.[42] A temperature jump beyond the spinodals results in a distinctly different transition mechanism referred to as spinodal decomposition. In this case, the energy barrier is gone and the initial phase becomes unstable. Consequently, the entire morphology transforms all at once, forming a final morphology without any long-range order. However, the C↔S spinodals are well removed from the C/S phase boundary (recall that the weak-segregation regime will be destroyed by fluctuations), and thus we would normally expect the nucleation and growth mechanism to occur. In fact, the S→C spinodal is not even accessible for compositions where $f<0.34$. Although this contradicts the experimental conclusions by Ryu *et al.*,[17,18] their indirect method of determining the spinodals cannot be considered completely reliable.

Our SCFT calculation models the transition as if the entire melt transforms all at once. Although this pathway should be closely related to a realistic transition, a nucleation and growth process would proceed much differently. For C→S, we expect that the transition is nucleated when one of the cylinders pinches off. After this irreversible step, a series of ruptures occurs in both directions transforming the cylinder into a row of spheres. Presumably this perturbs the neighboring cylinders causing them to break apart into spheres. Undoubtedly, spheres originating from different cylinders will be poorly correlated, and thus it will take some time for the bcc lattice to become well ordered. This is supported in scattering experiments by the temporary disappearance of scattering peaks during the transition.[20] The reverse transition, S→C, is presumably nucleated by the fusion of two spheres into an ellipsoid. Following that step, spheres start joining onto the two ends creating a long cylinder. The formation of one cylinder then directs the neighboring spheres to join together to form parallel cylinders. Both of these mechanisms suggest that the stable phase grows most rapidly along the direction of the cylinder axes.

Given the invariant polymerization index $\bar{N}$, Fig. 6(b)

provides the energy required to create a critical nucleus. This is also approximately the same energy required for each incremental step of the transition. If this energy was much larger than k_BT, we would expect a long incubation time for the formation of a critical nucleus, which would then grow very slowly. However, this energy is generally small and so the transition should proceed rapidly, although it may take a long time before the final phase becomes well ordered. In fact, at low segregations, the barrier becomes smaller than the energy k_BT of a typical thermal fluctuation. In this extreme case, the C and S phases cannot maintain their integrity and will be destroyed by fluctuations. This provides a convenient criterion for estimating the fluctuation effects on the ODT. For example, if $\bar{N}=10^4$, then we would expect the C/S boundary to be consumed by the disordered phase up to about $\chi N\approx 17$ ($f\approx 0.27$), whereas for $\bar{N}=10^3$, the disordered phase would extend up to $\chi N\approx 23$ ($f\approx 0.22$). Based on the standard Fredrickson–Helfand fluctuation correction,[13] symmetric block copolymer melts with $\bar{N}=10^4$ and 10^3 would be disordered up to $\chi N\approx 12.4$ and 14.6, respectively. Naturally, symmetric block copolymers would remain ordered to lower χN than asymmetric ones, but nevertheless this indicates that fluctuation effects are far more significant than previously anticipated. We note that our estimate should be the more reliable, as the Fredrickson–Helfand one uses an approximation valid only for $\bar{N}\gtrsim 10^6$.

As a transition is approached, the local minimum in the free energy surface becomes shallower resulting in pretransitional fluctuations. Using rheology, small-angle x-ray scattering (SAXS), and transmission electron microscopy (TEM), Ryu *et al.*[17,18] have examined these fluctuations for the C→S transition. According to their SAXS measurements, the fluctuations have a twinned bcc symmetry as expected. However, their TEM images reveal isolated grains exhibiting particularly strong pretransitional fluctuations, which is peculiar because the whole sample should fluctuate at a relatively uniform level. Nevertheless, this observation can be rationalized assuming their sample contained grains where the domain spacing was strained due to, for example, defects. Then, according to Fig. 10(b), these particular grains should exhibit larger fluctuations.

There are several previous theoretical approaches that we should note. Qi and Wang[28,29] have examined the free energy surface following paths determined by Cahn–Hilliard dynamics. They also restrict their consideration to paths where the morphology remains periodic. However, in this case, the periodicity, which results from the boundary conditions applied to their simulation box, is on a larger scale than that of the underlying morphology. Nevertheless, the periodicity seems to preclude the nucleation and growth mechanism, which is required for the system to overcome an energy barrier. In effect, the system is unable to create a single critical nucleus without simultaneously creating an infinite number of periodic images. Consequently, their calculation is limited to large temperature jumps beyond the spinodal limits where the initial phase becomes unstable.

Shi and co-workers,[30–32] on the other hand, make predictions by examining the local shape of the free energy surface about the various ordered phases. They expand the free energy to second-order in $\Phi(\mathbf{r})$, and infer the kinetic pathways based on the direction in which the free energy increases least rapidly. Although successful in many cases, there is a clear risk for misleading results. For example, there is no distinction between the correct direction and the opposite one leading away from the stable phase. Generally, the correct direction can be ascertained with common sense by just examining at how the morphology evolves in each case. However, things become far more complicated when the lowest energy mode is degenerate. In this case, the proper direction is some linear combination of the degenerate modes, the determination of which really requires an expansion to higher order, something that is generally not feasible. We attribute this difficulty to an incorrect suggestion by Laradji *et al.*[30] that the S→C transition involves some sort of complicated pathway, contrary to the experimental evidence.[16] This is strongly supported by the fact that we obtain the same S→C spinodal line as they do. The same problem may also apply to other transitions suggested by these authors.

Our calculation has the advantage that it examines an entire pathway between two phases, and it can do so regardless of whether the initial phase is metastable or unstable. Perhaps the most important advantage is that it can access the higher degrees of segregation characteristic of actual experiments. The previous calculations[28–32] have been limited to the weak-segregation regime, where the ordered phases are actually destroyed by thermal fluctuations. Naturally this precludes the weak-segregation calculations from providing quantitatively useful results, but they are also prone to qualitatively misleading predictions.[43] Although mean-field calculations in the strong- to intermediate-segregation regime are governed the simple interplay between the interfacial and stretching energies described in the Introduction,[6] weak-segregation calculations seem to behave somewhat differently.

V. CONCLUSIONS

We have located a low-energy pathway between the local minima, associated with hexagonally-packed cylinders and bcc spheres, in the Landau free energy surface for diblock copolymer melts. The pathway corresponds to an epitaxial transition where the domain spacing of the two phases is closely matched and where the cylinder axis is matched with the [111] direction of the bcc lattice. We evaluate the energy barriers, spinodal limits, and evolution of the morphology. The energy barrier is found to be remarkably small suggesting not only that the transition is rapid but also that fluctuations are more important than previously thought. Furthermore, the spinodal limits are well removed from the C/S phase boundary, implying that the transition proceeds by a nucleation and growth mechanism.

Based on past experiments and our present calculations, we can suggest a detailed description of the transition mechanism. In the C→S direction, the transition is nucleated by a single rupture in one of the cylinders. This initiates a further series of ruptures in both directions of the cylinder, transforming it into a series of spheres. Neighboring cylin-

ders do the same in a correlated manner such that the resulting spheres form one of two possible bcc lattices. Because of the low energy barrier, this step occurs rapidly. However, there will be a considerable laps before a well-defined bcc ($Im\bar{3}m$) symmetry emerges due to a weak correlation between the rupturing cylinders. In the S→C direction, the process is simply reversed. The nucleation occurs when two spheres fuse together forming an ellipsoid. Spheres continue to join onto the ends transforming it into a cylinder oriented along one of the diagonal directions of the bcc unit cell. The initial cylinder then guides the fusion of neighboring spheres producing parallel cylinders with a hexagonal packing. Again, this transition should be rapid due to the small energy barrier involved. Both C↔S epitaxial transitions rely on a fortuitous match in the domain spacings of the C and S phases. As long as there is only a small mismatch, the domain spacing should adjust as the transition proceeds. On the other hand, a large mismatch may leave the final phase with a nonequilibrium domain size, that will take a long time to equilibriate.

Our study offers explanations for several experimental results, but raises questions regarding others. For example, the *memory* effect observed by Kimishima *et al.*[16] regarding the cylinder orientation in the phase sequence C→S→C is attributed to the poor correlation between spheres originating from different cylinders. This lack of correlation also explains the temporary loss of long-range order observed in the SAXS experiments of Krishnamoorti *et al.*[20] as C transforms to S. Furthermore, the highly nonuniform pretransitional fluctuations in the C phase observed by Ryu and Lodge[17] can be attributed to defeats causing variations in the domain size. Although some experiments[16–18] observe SAXS results consistent with the proposed epitaxy, others[15,20] do not. A possible explanation is that their C phase contained two cylinder orientations, which is supported by results in Ref. 40. Although Refs. 17 and 18 suggest the existence of a S→C spinodal contrary to our predictions, we feel their evidence is not particularly compelling. Needless to say, further experiments would be very useful, not only to resolve the above issues, but also to address other important issues such as the effects of a domain spacing mismatch. The understanding we develop from this C↔S transition will certainly apply to the other order–order transitions in block copolymer melts as well as perhaps those in various liquid crystal and biological systems.

ACKNOWLEDGMENTS

We are grateful to An-Chang Shi for discussions regarding calculations in Refs. 30 and 31. This work was supported by the EPSRC (GR/M61160).

[1] F. S. Bates and G. H. Fredrickson, Phys. Today **52**, 32 (1999).
[2] M. W. Matsen and F. S. Bates, Macromolecules **29**, 1091 (1996).
[3] M. W. Matsen and F. S. Bates, Macromolecules **29**, 7641 (1996).
[4] L. Leibler, Macromolecules **13**, 1602 (1980).
[5] A. N. Semenov, Sov. Phys. JETP **61**, 733 (1985).
[6] M. W. Matsen and F. S. Bates, J. Chem. Phys. **106**, 2436 (1997).
[7] D. A. Hajduk, H. Takenouchi, M. A. Hillmyer, F. S. Bates, M. E. Vigild, and K. Almdal, Macromolecules **30**, 3788 (1997).
[8] E. L. Thomas, D. J. Kinning, D. B. Alward, and C. S. Henkee, Macromolecules **20**, 2934 (1987).
[9] J. K. Kim, H. H. Lee, M. Ree, K.-B. Lee, and Y. Park, Macromol. Chem. Phys. **199**, 641 (1998).
[10] N. Sakamoto and T. Hashimoto, Macromolecules **31**, 8493 (1998).
[11] C. D. Han, N. T. Vaidya, D. Kim, G. Shin, D. Yamaguchi, and T. Hashimoto, Macromolecules **33**, 3767 (2000).
[12] S. A. Brazovskii, Sov. Phys. JETP **41**, 85 (1975).
[13] G. H. Fredrickson and E. Helfand, J. Chem. Phys. **87**, 697 (1987).
[14] S. Sakurai, H. Kawada, T. Hashimoto, and L. J. Fetters, Macromolecules **26**, 5796 (1993).
[15] K. A. Koppi, M. Tirrell, F. S. Bates, K. Almdal, and K. Mortensen, J. Rheol. **38**, 999 (1994).
[16] K. Kimishima, T. Koga, and T. Hashimoto, Macromolecules **33**, 968 (2000).
[17] C. Y. Ryu and T. P. Lodge, Macromolecules **32**, 7190 (1999).
[18] C. Y. Ryu, M. E. Vigild, and T. P. Lodge, Phys. Rev. Lett. **81**, 5354 (1998).
[19] S. Sakurai, T. Hashimoto, and L. J. Fetters, Macromolecules **29**, 740 (1996).
[20] R. Krishnamoorti, A. S. Silva, M. A. Modi, and B. Hammouda, Macromolecules **33**, 3803 (2000).
[21] M. A. Modi, R. Krishnamoorti, M. F. Tse, and H.-C. Wang, Macromolecules **32**, 4088 (1999).
[22] R. Krishnamoorti, M. A. Modi, M. F. Tse, and H.-C. Wang, Macromolecules **33**, 3810 (2000).
[23] C. Y. Ryu, M. S. Lee, D. A. Hajduk, and T. P. Lodge, J. Polym. Sci., Part B: Polym. Phys. **35**, 2811 (1997).
[24] J. K. Kim, H. H. Lee, Q.-J. Gu, T. Chang, and Y. H. Jeong, Macromolecules **31**, 4045 (1998).
[25] P. Sakya, J. M. Seddon, R. H. Templer, R. J. Mirkin, and G. J. T. Tiddy, Langmuir **13**, 3706 (1997).
[26] M. W. Matsen, Phys. Rev. Lett. **80**, 4470 (1998).
[27] Z.-G. Wang, Curr. Opin. Colloid Interface Sci. **3**, 428 (1998).
[28] S. Qi and Z.-G. Wang, Phys. Rev. Lett. **76**, 1679 (1996); Phys. Rev. E. **55**, 1682 (1997); J. Chem. Phys. **111**, 10681 (1999).
[29] S. Qi and Z.-G. Wang, Polymer **39**, 4639 (1998).
[30] M. Laradji, A.-C. Shi, J. Noolandi, and R. C. Desai, Macromolecules **30**, 3242 (1997).
[31] M. Laradji, A.-C. Shi, R. C. Desai, and J. Noolandi, Phys. Rev. Lett. **78**, 2577 (1997); M. W. Matsen *ibid.* **80**, 201 (1998).
[32] A.-C. Shi and J. Noolandi, Polymer **39**, 4649 (1998); A.-C. Shi, J. Phys.: Condens. Matter **11**, 10183 (1999).
[33] M. F. Schultz, F. S. Bates, K. Almdal, and K. Mortensen, Phys. Rev. Lett. **73**, 86 (1994).
[34] M.E. Vigild, K. Almdal, K. Mortensen, I. W. Hamley, J. P. A. Fairclough, and A. J. Ryan, Macromolecules **31**, 5702 (1996); G. Floudas, R. Ulrich, U. Wiesner, and B. Chu, Europhys. Lett. **50**, 182 (2000).
[35] E. Helfand, J. Chem. Phys. **62**, 999 (1975).
[36] M. W. Matsen and F. S. Bates, J. Polym. Sci., Part B: Polym. Phys. **35**, 945 (1997).
[37] *International Tables for X-Ray Crystallography*, edited by N. F. M. Henry and K. Lonsdale (Kynoch, Birmingham, 1969).
[38] A.-C. Shi, J. Noolandi, and R. C. Desai, Macromolecules **29**, 6487 (1996).
[39] F. S. Bates, M. F. Schulz, A. K. Khandpur, S. Förster, J. H. Rosedale, K. Almdal, and K. Mortensen, Faraday Discuss. **98**, 7 (1994).
[40] T. Tepe, M. F. Schulz, J. Jhao, M. Tirrell, and F. S. Bates, Macromolecules **28**, 3008 (1995).
[41] M. F. Schulz (private communication).
[42] The energy barrier to form the initial nucleus should be somewhat larger than that of the subsequent steps, and thus an overall decrease in the barriers should have a greater effect on the production of nuclei than the growth rate of the resulting grains.
[43] M. W. Matsen, J. Chem. Phys. **107**, 8110 (1997); D. Duque and M. Schick *ibid.* **113**, 5525 (2000); M. W. Matsen (unpublished).